Imaging and Inverse Problems of Partial Differential Equations

F. Natterer
Institut für Numerische und Angewandte Mathematik
Westf. Wilhelms-Universität Münster
Einsteinstrasse 62, D-48149 Münster, Germany
e-mail: nattere@math.uni-muenster.de

April 6, 2006

1 Introduction

"Mathematical Imaging" is a notion that was unknown in the mathematical world of the 70-ties of the last century. By now it has become a lively mathematical discipline. Mathematical Imaging comprises image processing (often considered as part of engineering), image understanding (part of artificial intelligence) and image reconstruction (generating images from data produced by specifically designed devices). This paper deals with this last kind of imaging, i.e. with techniques such as X-ray computed tomography, emission tomography, near infrared imaging, electrical impedance tomography, seismic imaging, radar, and ultrasound tomography. This list is necessarily incomplete. New imaging modalities come up every fortnight.

Many image reconstruction problems can be formulated as inverse problems of partial differential equations. It is this point of view that we adopt in this note. The goal is a unified theory of image reconstruction. It turns out that a large class of reconstruction algorithms can be formulated independently of the type of the underlying differential equation and were known in the respective fields of applications previously under various names. Likewise the structure of exact and approximate inversion formulas (if available)

is surprisingly similar. On the other hand the quality of the reconstructed image can often be predicted simply from the type of the underlying differential equation.

The plan of the paper is as follows: We start with three techniques (X-ray tomography (CT), single particle emission tomography (SPECT) and positron emission tomography (PET)) that are based on the transport equation. We demonstrate the advantage of the differential equations point of view over the traditional integral geometric approach by accurate modelling (scatter) and new inversion formulas (Novikov). As a further example for the transport equation we discuss near infrared imaging (NIR), where we will make the transitions to elliptic equations by the diffusion approximation. Another example for imaging with elliptic equations is electrical impedance tomography (EIT). We conclude the paper with seismic imaging, synthetic aperture radar (SAR) and ultrasound tomography which are governed by the wave equation.

2 X-ray tomography (CT)

Even though elementary mathematical methods were used in imaging well before the 70-ties (e.g. in seismics and radar), the advent of CT in 1973 was the beginning of the new mathematical discipline of imaging. It lead to a mathematical sophistication that was unheard of in imaging before.

The principle of CT is nowadays well known; see Figure 1. A thin X-ray beam scans a cross section of the human body, and a computer produces an image. A modern CT scanner is shown in Figure 2. In Figure 3 we see the data measured in the scanning process and the reconstructed image.

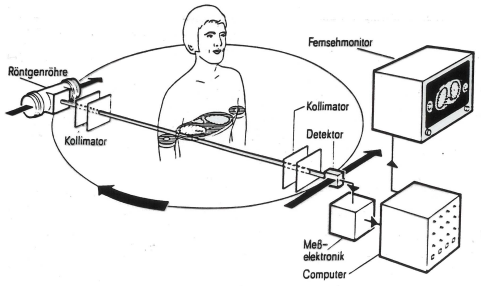

Figure 1: Principle of Computerized Tomography (CT).

Figure 2: Modern CT scanner.

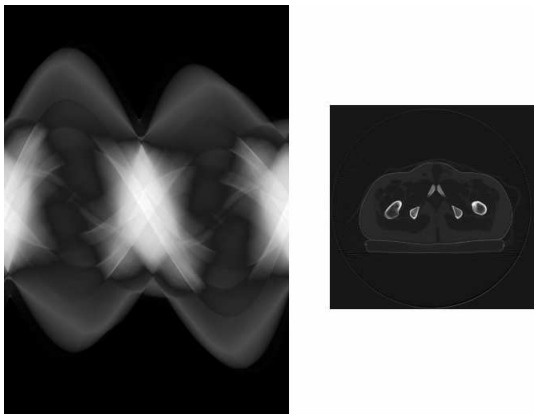

Figure 3: Data set (left) for an abdominal cross section (right). Note that the discontinuities in the cross section can clearly be seen in the data set.

The most simple mathematical model of CT assumes that the scanner measures the line integrals of the absorption coefficient $f(x)$. This gives rise to the Radon transform

$$(Rf)(\theta, s) = \int\limits_{x\cdot\theta=s} f(x)dx, \quad \theta \in S^1, s \in \mathbb{R}^1$$

and the mathematical problem is to invert R. In principle this was solved by Radon's 1917 inversion formula

$$f = R^* K g, \quad g = Rf \tag{2.1}$$

where R^* is the backprojection (the adjoint of R),

$$(R^*g)(x) = \int_{S^1} g(\theta, x \cdot \theta) d\theta$$

and K the composition of the derivative and the Hilbert transform:

$$(Kg)(s) = \frac{1}{4\pi^2} \int \frac{g'(t)}{s-t} dt.$$

The early history of CT has still to be written. For a preliminary account see [25]. The works [15] - [19] can serve as an introduction into the mathematical and technical aspects of CT.

The most important reconstruction algorithm, the filtered backprojection algorithm, can be viewed as a computer implementation of Radon's inversion formula. In the first commercially available CT scanner an iterative method was used which is based on Kaczmarz's 1937 method for solving linear systems of equations. Its update is

$$f \leftarrow f - \alpha R_\theta^* C_\theta^{-1} (R_\theta f - g_\theta) \tag{2.2}$$

where

$$g_\theta = g(\theta, \cdot), \quad R_\theta f = (Rf)(\theta, \cdot)$$

C_θ is a certain positive definite operator and α is a relaxation parameter. All of the iterative reconstruction methods in this paper are patterned after (2.2).

Research in the mathematics of CT is still going on. As an example I mention truly 3-D-cone-beam CT, with the X-ray source on a helix and 2D detector arrays. Katsevich's algorithm [26] is among the most competitive ones, see Figure 4. The computational bottleneck is the backprojection which still needs a speed up. Ideas include divide-and-conquer strategies and non-equidistant fast Fourier transforms (FFT's).

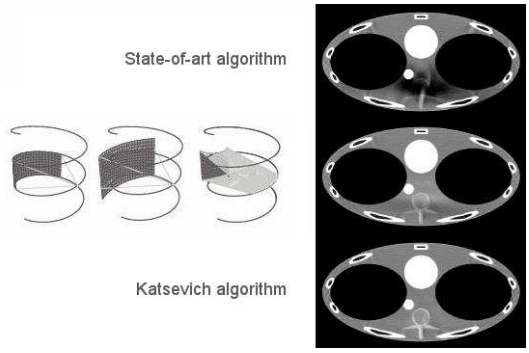

Figure 4: Scanning geometry (left) and reconstructions (right) with different reconstruction algorithms for helical scanning.

3 CT as an inverse problem of the transport equation

After these introductory remarks we come to the main topic of this paper. We formulate CT as an inverse problem for the transport equation. Introducing the density $u(x,\theta)$ of the particles at $x \in \Omega$ travelling in direction $\theta \in S^1$ we have in $\Omega \times S^1$

$$\theta \cdot \nabla u(x,\theta) + f(x)u(x,\theta) = \delta(x-x_0)\delta(\theta-\theta_0) \tag{3.1}$$

and, in the absence of exterior radiation,

$$u(x,\theta) = 0, \quad x \in \partial\Omega, \quad \theta \cdot \nu_x \leq 0 \tag{3.2}$$

with ν_x the exterior normal at $x \in \partial\Omega$. (3.1), (3.2) is a reasonable problem that admits a unique solution under natural conditions. The inverse problem of CT consists in finding f from

$$u(x,\theta), \quad x, x_0 \in \partial\Omega, \quad \theta = (x-x_0)/|x-x_0|.$$

The inverse problem reduces immediately to the Radon transform since

$$u(x,\theta) = H((x-x_0)\cdot\theta)\delta((x-x_0)\theta^{\perp})\delta(\theta-\theta_0)e^{\int_{x_0}^{x} f ds}.$$

This (trivial) example has already the main ingredients of imaging and partial differential equations: The underlying physical process is described by the partial differential equation, and the measurements give rise to boundary values of the solution. From this overdeterminicity the model parameters (in this case the X-ray absorption f) have to be determined. Integral geometry comes in only because integral geometric transforms (in this case the Radon transform) are exact (or approximate) solution operators.

4 Single particle emission computed tomography (SPECT)

Now we consider the transport equation

$$\theta \cdot \nabla u(x,\theta) + a(x)u(x,\theta) = f(x) \quad \text{in} \quad \Omega \times S^1 \tag{4.1}$$

$$u(x,\theta) = 0, \quad x \in \partial\Omega, \quad \theta \cdot \nu_x \leq 0. \tag{4.2}$$

(4.1), (4.2) describes SPECT: A radiopharmaceutical is injected and the radiation is measured outside the body in a tomographic fashion, see Figure 5. One seeks the distribution f of the radiopharmaceutical. We pose two inverse problems:

Inverse problem 1:	Assume a to be known. Find f from $u(x,\theta)$, $x \in \partial\Omega$, $\theta \in S^1$.
Inverse problem 2:	Find a and f from $u(x,\theta)$, $x \in \partial\Omega$, $\theta \in S^1$.

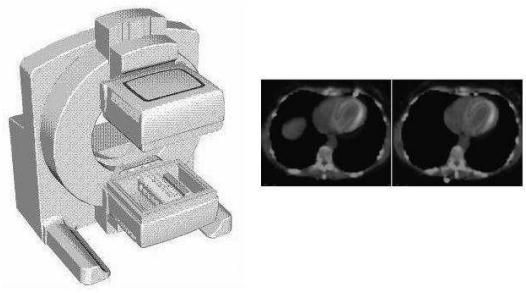

Figure 5: Novel SPECT scanner (Solstice of Philips Medical Systems) (left) and state-of-the-art reconstructions (right) of thorax.

Inverse problem 1 (a so-called inverse source problem) is linear. It corresponds to the case in which the attenuation a of the body is known. Inverse problem 1 reduces to the attenuated Radon transform

$$(R_a f)(\theta, s) = \int_{x\cdot\theta=s} f(x) e^{-\int_a^\infty a(x+s'\theta)ds'} dx \tag{4.3}$$

since the solution of (4.1), (4.2) is

$$u(x,\theta) = \int_{-\infty}^0 f(x+s\theta) e^{\int_a^\infty a(x+s'\theta)ds'} ds$$

which is just a reparameterization of (4.3). R_a admits an explicit inversion formula very similar to Radon's inversion formula: It $g = R_a f$, then

$$f = \frac{1}{4\pi} Re\ div R^*_{-a}(\theta e^{-h} H e^h g) \tag{4.4}$$

where H is the Hilbert transform, $h = 1/2(I+iH)Ra$ and R_a^* is the (weighted) backprojection

$$\begin{array}{lcl} (R_a^* g)(x) & = & \int_{S^1} e^{-(Da)(x,\theta^\perp)} g(\theta, x\cdot\theta) d\theta \\ (Da)(x,\theta) & = & \int_0^\infty a(x+s\theta) ds. \end{array}$$

This formula was obtained by Novikov [32] in 2000. In our context it is interesting to note that Novikov received his result by working directly on (4.1), (4.2) (by the $\overline{\partial}$-method), rather than dealing with the integral geometric counterpart R_a. Later simpler derivations of (4.4) (most notably in [33] were found. However it is very unlikely that (4.4) would have been found without the differential equation viewpoint.

Inverse problem 2 is non linear. It is not uniquely solvable. However if a is modelled by a few parameters, these parameters can be determined in favourable circumstances. This is possible since consistency conditions in the range of R_a are known; see [40].

5 Positron emission tomography (PET)

In PET we also determine the density f of a radiopharmaceutical inside the body. The underlying physics is different from SPECT in that the sources eject the particles pairwise in opposite directions, and the detectors work in

coincidence mode, i.e. particles are counted only if they arrive at the same time. Often the particles are scattered before they arrive at the detector. For accurate modelling of the scatter the simple transport equations of the previous sections have to be complemented by a scattering integral:

$$\theta \cdot \nabla u(x,\theta) + a(x)u(x,\theta) = \int_{S^2} k(x,\theta,\theta')u(x,\theta')d\theta' + f(x)$$

where $k(x,\theta,\theta')$ is the provability that a particle arriving at x with direction θ' continues its trip in direction θ. For simplicity we ignore the change of energy in the scattering process. Assuming a, k known we again want to find f from measurements of $u(x,\theta)$ at the boundary of the reconstruction region Ω. For a probabilistic derivation of the measurement operator see [27].

6 Near infrared imaging (NIR)

So far we discussed established imaging techniques that are available in major hospitals. Now we come to techniques that are still under development. Human tissue is opaque for visible light, but becomes transparent in the NIR regime. The differential equation is again a transport equation:

$$\theta \cdot \nabla u(x,\theta) + (\mu_s(x) + \mu_a(x))u(x,\theta) = \mu_s(x) \int_{S^2} k(x,\theta,\theta')u(x,\theta')d\theta' + \delta(x-y)$$

Here $y \in \partial\Omega$ is the position of a laser source (700 - 1000 nm), k a known scattering kernel, and μ_s, μ_a the scattering and attenuation coefficients, respectively. Again the problem is to recover μ_s, μ_a from measurements of $u(x,\theta)$ for $x, y \in \partial\Omega$.

In NIR, the scattering phenomena by far exceed the effects of transport: The mean free path is smaller than 0.01 mm. Thus the transport equation can be replaced by the diffusion approximation: Putting

$$u(x) = \int u(x,\theta)d\theta$$

and using time harmonic illumination with frequency ω we obtain to good accuracy

$$-\nabla \cdot (D(x)\nabla u(x)) + (\mu_a(x) + i\frac{\omega}{c})u(x) = 0, \quad D = \frac{1}{3(\mu_a + \mu_s')} \tag{6.1}$$

where c is the speed of light and μ_s' the reduced scattering coefficient. The boundary conditions become

$$u(x) + 2D(x)\frac{\partial u}{\partial v}(x) = g^-(x) \qquad (source) \tag{6.2}$$

$$\frac{\partial u}{\partial v}(x) = g(x) \qquad (measurement) \tag{6.3}$$

The inverse problem consists in finding μ_a and D from the measurements at the boundary.

Numerically the inverse problem is of the following form: Suppose we have p sources $g_j^-, j = 1, \ldots, p$. Let u_j be the corresponding solution of (6.1), (6.2), and put

$$R_j(f) = \frac{\partial u_j}{\partial v}, \quad f = \begin{pmatrix} D \\ \mu_a \end{pmatrix}.$$

Then we have to solve the nonlinear system

$$R_j(f) = g_j, \quad j = 1, \ldots, p. \tag{6.4}$$

An approximate solution of (6.4) can be found by an immediate extension of (2.2):

$$f \leftarrow f - \alpha(R_j'(f))^*(R_j(f) - g_j) \tag{6.5}$$

where R_j' is the derivative of R_j. The operator $(R_j'(f))^*$ can be computed by adjoint differentiation:

$$(R_j'(f))^* r = \begin{pmatrix} -\nabla u_j \cdot \nabla \overline{z} \\ -u_j \overline{z} \end{pmatrix} \tag{6.6}$$

where z is the solution of

$$-\nabla \cdot (D\nabla z) + (\mu_a + i\frac{\omega}{c})z = 0 \quad \text{in} \quad \Omega, \quad z = \overline{r} \quad \text{on} \quad \partial\Omega. \tag{6.7}$$

The reconstruction process (6.5) - (6.7) reveals the following scheme: Phase conjugate and backpropagate the residual $r = R_j(f) - g_j$, phase conjugate the backpropagated field z and correlate it with the true field u_j to produce the update for f. The phase conjugations are nothing but time reversal in frequency domain.

7 Electrical impedance tomography (EIT)

Another example of an imaging technique that is based on an elliptic equation is EIT. Here the differential equation is

$$\nabla \cdot (\sigma \nabla u) = 0 \quad \text{in} \quad \Omega \tag{7.1}$$

with $\sigma = \sigma(x)$ the conductivity. On the boundary ∂ *Omega* we have

$$\frac{\partial u}{\partial v} = f, \quad u = g. \tag{7.2}$$

One of these quantities is prescribed, the other one is measured. The inverse problem calls for determining σ from many pairs f, g.

EIT has found much interest in mathematical circles. Calderon [6] proved uniqueness for the linearized problem, introducing the by now famous method of exponentially growing solutions. This method was extended by Nachmann [21], Sylvester-Uhlmann [37] to various cases of the fully nonlinear problem and even lead to numerical methods [20].

Being based on an elliptic equation, EIT suffers from the same shortcomings as NIR imaging. For what can be achieved see [7].

8 Seismic imaging

In the rest of the paper we deal with imaging techniques that are based on the wave equation. In a common source gather the acoustic pressure $u(x,t)$ is measured at each point x on the surface $x_n = 0$ for each source s on the surface. u satisfies

$$\begin{array}{lcl} \frac{\partial^2 u}{\partial t^2} & = & c^2(x)(\Delta u + q(t)\delta(x-s)) \quad \text{in} \quad x_n > 0, \\ u & = & 0 \quad \text{for} \quad t < 0. \end{array} \tag{8.1}$$

Here, $c(x)$ is the speed of sound in the subsurface $x_3 > 0$ and q the source wavelet. The inverse problem consists in computing c from the seismograms $u(x,t),\ x_3 = 0, \quad t \geq 0$.

Most imaging in seismics and is done as high frequency imaging. By this we mean that c is decomposed as $c = c_0 + c_1$ where c_0 is a smooth, i.e. slowly varying background that is known , and c_1 is a small highly oscillating function, representing the sought for fine structure of the subsurface.

High frequency imaging is based on linearization: We approximately have

$$R_s(c) \approx R_s(c_0) + R_s'(c_0)c_1.$$

Using the data $g_s = R_s(c)$, applying the adjoint of the derivative $R_s'(c_0)$ and integrating over the sources we obtain

$$\int (R_s'(c_0))^*(g_s - R_s(c_0))ds = Fc_1, \qquad F = \int (R_s'(c_0))^* R_s'(c_0)ds. \tag{8.2}$$

The important fact is that F is an elliptic pseudo differential operator [2]. Such operators preserve the singular support of a function. Thus the left hand side of (8.2) which can be computed from the data (if c_0 is known) has precisely the same discontinuities as c_1. Hence it provides a true picture of the fine structure of the subsurface.

High frequency imaging as described above works well in practice - provided a good estimate for c_0 is available. Finding good estimates for c_0 is known as the velocity estimation problem is seismic imaging.

For the evaluation of (8.2) we have to compute $(R_s'(c_0))^* r$ for r a seismogram. One can show that

$$(R_s'(c_0))^* r = \frac{2}{c_0} \int_0^T \frac{\partial^2 u}{\partial t^2} z dt \tag{8.3}$$

where u is the pressure field for c_0 (i.e. the solution of (8.1) for $c = c_0$) and z is the solution of

$$\begin{array}{lcl} \frac{\partial^2 z}{\partial t^2} & = & c_0^2 \Delta z \quad \text{in} \quad x_3 > 0, \\ z & = & 0, \quad \frac{\partial z}{\partial x_3} = -\frac{r}{c_0^2} \quad \text{on} \quad x_3 = 0, \\ z & = & 0 \quad \text{for} \quad t > T. \end{array} \tag{8.4}$$

Note that (8.4) is a final value problem. In the light of (8.3), (8.4), the reconstruction formula (8.2) can be viewed as time reversal [12]: Backpropagate the residual $r = g_s - R_s(c_0)$ through the medium and correlate it with the pressure field.

The left hand side of (8.2) is clearly reminiscent of the update in the iterative methods (2.2) and (6.5). It is tempting to use iterative approach also for the seismic problem, iterating according to

$$c \leftarrow c - \alpha (R_s'(c))^* (R_s(c) - g_s). \tag{8.5}$$

Such methods have been widely used [39], [5], with very limited success. In order to understand what's going on we employ Fourier analysis, under the simplifying assumptions

(i) $c^2(x) = c_0^2/(1 + f(x))$, f small, c_0 constant.

(ii) The sources s are fired simultaneously (so as to produce a plane wave travelling in the x_3 direction).

Then one can show [23] that the data determine the function

$$\hat{q}(\omega)\hat{f}(\xi', -k - \sqrt{k^2 - |\xi'|^2}), \quad k = \frac{\omega}{c_0} \tag{8.6}$$

where $\hat{q}$, $\hat{f}$ are the 1D and 3D Fouriertransforms of q, f, respectively. Now assume that the source wavelet q has frequencies in $[\omega_0, \omega_1]$, i.e. $\hat{q}(\omega)$ in $[\omega_0, \omega_1]$ and put $k_0 = \omega_0/c_0$, $k_1 = \omega_1/c_0$. Then the domain where $\hat{f}$ is determined is sketched in Fig.7.

The range (k_0, k_1) of available wave numbers depends entirely on the source wavelet q. For $q = \delta$, the Dirac δ-function, $k_0 = 0$ and $k_1 = \infty$. In this case we conclude from Fig. 7 that a layered medium with dip angle $< \pi/4$ can be well reconstructed by a single downgoing plane wave, and that an arbitrary medium can be reconstructed from two plane waves making an angle of $\pi/2$. In view of [36] this is not surprising. Unfortunately such a wavelet is not supported by the earth. For real wavelets, such as the Ricker wavelet, the range of usable wave numbers is restricted to a finite interval $[k_0, k_1]$. Typically, $k_0 = k_1/10$. In that case the part $|\xi| < k_0$ of $\hat{f}(\xi)$ can not be recovered, not even from plane waves of arbitrary directions.

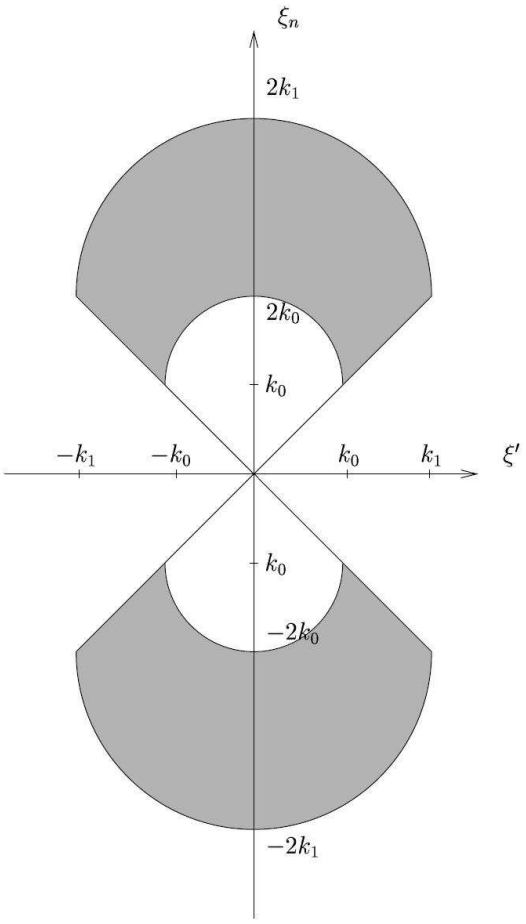

Figure 7: Region in Fourier domain where $\hat{f}$ is determined by the data generated by a plane wave falling in from top.

Thus we see that the low frequency parts of f (and hence of c) are not determined by the data. A method such as (8.5) which by its very nature tries to determine these low frequency parts is bound to fail. This failure is entirely due to the missing low frequencies in the source wavelet q.

Estimating the low frequency part of the velocity can be viewed as the most important problem in seismic imaging. A promising technique is to exploit the overposedness of seismic data [38].

Imaging with the wave equation has recently found an extension to random media [35]. Even though the theoretical background is quite different from the deterministic setting above, backpropagation and time reversal still

play an important role.

9 Synthetic aperture radar (SAR)

SAR is another instance of imaging with the wave equation where high frequency methods play a dominant role. the geometry of SAR is explained in Figure 6: A plane is flying over a terrain that is described by the ground reflectivity function $f(x_1, x_2)$. An antenna on the plane sends out a radar signal and measures the returned impulse. From these measurements along the flight track f has to be reconstructed.

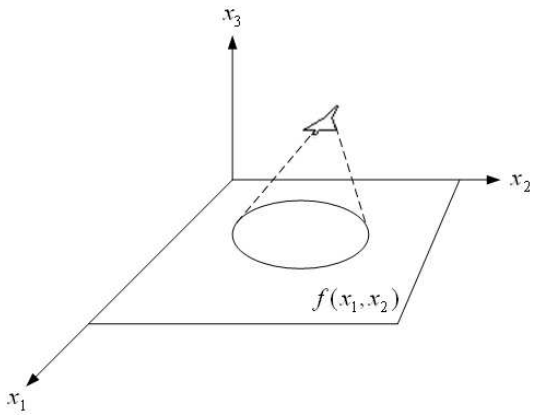

Figure 6: SAR geometry. Data are collected along the flight path.

In the most simple case f is reconstructed from its averages over circles whose midpoints are on the flight track [1], [17]. In a more refined model the propagation of the signal is described by the wave equation

$$\frac{\partial^2 u}{\partial t^2} = c^2(\Delta u + q(t)\delta(x-y))$$

where y is a point on the flight track, $q(t) = e^{i\omega t}$ the time harmonic excitation of the antenna, and

$$\frac{1}{c^2} = \frac{1}{c_0^2} + f(x_1, x_2)\delta(x_3)$$

with c_0 the speed of light. The inverse problem consists in finding f from $u(y,t)$ for y on the flight track and $t > 0$.

By linearising around $f = 0$ (Born approximation) and the far field approximation (y is far away from the support of f) one can show that approximately [8]

$$u(y,t) = u_0(y,t) + \frac{\omega^2 e^{i(\omega t + 2k|y|)}}{16\pi^2|y|^2} \int f(x) e^{-2ik\frac{y}{|y|}\cdot x} dx$$

where $k = \omega/c_0$ is the wave number and u_0 is the (known) field for $f = 0$. k is restricted to an interval $[k_1, k_2]$ much shorter than the central wave number $(k_1 + k_2)/2$.

Thus the problem amounts to determining f from its Fourier transform $\hat{f}(2ky/|y|)$. Since k is very large and $y/|y|$ is restricted to a small angular range (typically a few degrees) we only obtain $\hat{f}$ in a small truncated sector far away from the origin.

It is clear that from so little information f can not be reconstructed uniquely. However, microlocal analysis [30] shows that essential features of f such as corners can be recovered. Another difficulty is computational: In order to find f from $\hat{f}$ one has to perform a fast Fourier transform (FFT). The usual FFT algorithm require $\hat{f}$ to be known on a cartesian grid, what is clearly not the case here. Thus non-equidistant FFT's [13] or gridding techniques [4] have to be used.

10 Ultrasound transmission tomography

In the two preceding sections we have seen that wave equation imaging using only reflected signals suffers from a serious drawback: It is difficult to recover low frequency features. Thus most of the work in seismic and radar imaging is high frequency. Present day's medical ultrasound is also based on reflections.

The situation changes completely if transmitted signals are available. This is the case in novel medical ultrasound scanners; see Figure 8. We analyze the impact of transmission measurements again in Fourier domain; see Figure 9. To fix ideas we take $n = 2$. The combined reflection and transmission signals determine $\hat{f}$ in the disc around $(0, k_1)$ of radius k_1, minus the disk around $(0, k_0)$ with radius k_0. This is the picture for one downgoing plane wave.

Figure 8: Ultrasound scanner developed by TechniScan, Salt Lake City (left), scanning geometry (top right) and reconstruction of speed of sound and attenuation (bottom right).

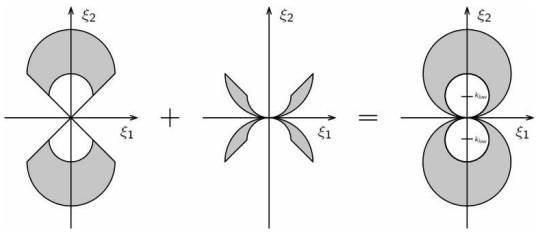

Figure 9: Regions in Fourier span where $\hat{f}$ is determined by reflection (left) and transmission (middle) from a single plane wave. Combined region is also shown (right).

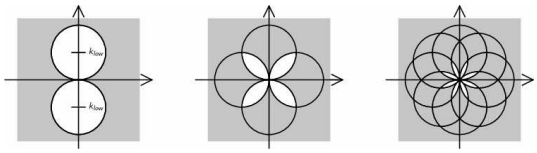

Figure 10: Regions in Fourier domain in which $\hat{f}$ is determined by one (left), two (middle) and four (right) plane waves.

Now let $k_1 \to \infty$ and use two plane waves making an angle of 90° and four plane waves making angles of 45°. Then we get the pictures in Figure 10. We see that for a modest number of plane waves we get on almost complete coverage in Fourier space. Of course this is a classical result [3]. As in the previous sections this rigoursly holds only in the Born approximation, i.e. if

the scattering is weak. However practical experience suggests that it is also true for fairly strong scattering.

As image reconstruction algorithm for ultrasound transmission tomography one can use the algorithm (8.5). Since the number of sources is large a preprocessing step (plane wave stacking [23]) is necessary to keep the computation time low. Alternatively one can work in frequency domain. This leads to the following inverse problem for the Helmholtz equation:

Let u be the solution of

$$\begin{aligned} \Delta u + k^2(1+f(x))u &= 0 \quad \text{in} \quad \mathbb{R}^2, \\ u &= e^{ikx\cdot\theta} + u_s \end{aligned} \tag{10.1}$$

where $\theta \in S^1$ and u_s satisfies the Sommerfeld radiation condition. f is the complexe valued function

$$f = \frac{c_0^2}{c^2} - 1 - \frac{i}{k}\frac{2\alpha c_0}{c} \tag{10.2}$$

where $c(x)$ is the local speed of sound, c_0 the speed of sound in the ambient medium, and α is the attenuation coefficient. f is supported in $|x| \leq r$. Find f from the values of $u_s(x)$ for $|x| = r$, k fixed, and $\theta \in S^1$.

Again the problem is easily solved in the Born approximation, and there even exists an explicit error estimate [24]. In the Born approximation $\hat{f}$ is stably determined by the data in a circle of radius $2k$. According to the Shannon sampling theorem this means that f can be stably determined with spatial resolution π/k. As has been shown recently [34] this is true also for the fully nonlinear problem.

Unfortunately the Born approximation is not applicable to medical imaging, since f is far too big. Even though explicit methods based on the $\overline{\partial}$ technique exist [31] the methods of choice seem to be iterative, patterned after (2.2), (6.5), (8.5). These methods require the repeated solution of the boundary value problem (10.1) and its time-reversed analogue. Since k is large this is a challenge in itself, quite independently of the inversion process.

A way out is the reformulation of the boundary value problem (10.1) as an initial value problem. This sounds like heresy, since initial value problems for elliptic equations are notoriously unstable. However a closer analysis shows that this instability is a pure high frequency phenomenon that concerns only spatial frequencies beyond k. These are irrelevant if we restrict the spatial

resolution of the reconstructed image to π/k, i. e. one half of the wavelength of the irradiating plane wave. For the stability of the initial value problem for the Helmholtz equation see [28], [18]. Highly efficient marching schemes for the initial value problem for the Helmholtz equation are described in [29].

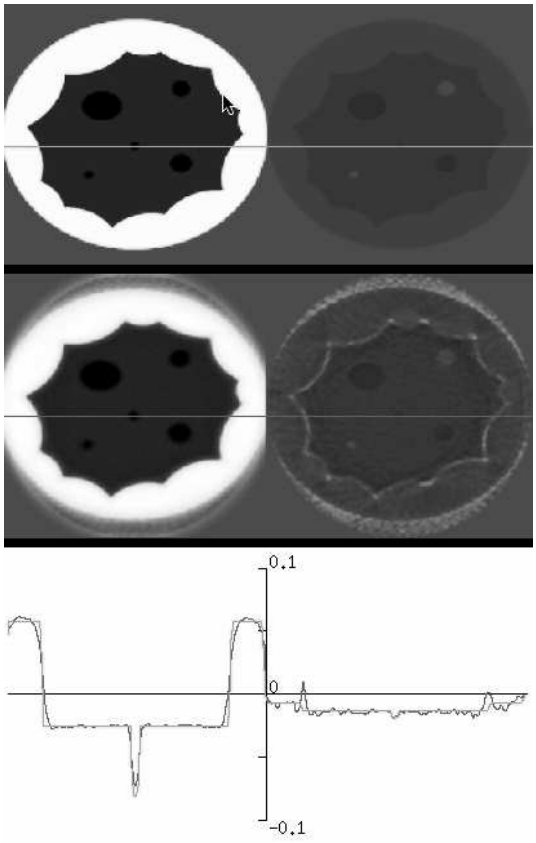

Figure 11: Top: Real (left) and imaginary (right) part of breast phantom. Middle: Reconstructions. Bottom: Cross section through phantom and reconstruction along the horizontal line displayed above.

What can be achieved by these techniques is shown in Figure 11. The computations are done on a 256×256 grid and require about 1 minute on a 3 GHz double processor PC.

For k small, the resolution is poor. However one can still detect sufficiently large objects. This can be done by various methods of inverse obstacle scattering [9], [16]. This works with methods that are completely different from those discussed in this paper.

References

[1] Anderssen, L.E.: In the determination of a function from spherical averages, SIAM J. Math. Anal. **19**, 214-232 (1988).

[2] Beylkin, G.: Imaging of discontinuities in the inverse scattering problem by inversion of a causal generalized Radon transform, J. Math. Phys. **26**, 99 - 108 (1985).

[3] Born, M. and Wolf, E.: Principle of Optics. Pergamon Press, London 1980.

[4] Brouw, W. N.: Aperture synthesis, Methods Comput. Physics. **B14**, 131 - 175 (1975)

[5] Bunks, C., Saleck, F. M., Zaleski, S. and Chavent, G.: Multiscale waveform inversion, Geophysics **60**, 1457-1473 (1995).

[6] Calderon, A. B.: On an inverse boundary value problem, in: Seminar on Numerical Analysis and its Application to Continuum Physics, 65-73, Soc. Brasileira de Matematica, Rio de Janeiro (1980).

[7] Cheney, M., Isaacson, D. and Newell, I. C.: Electrical impedance tomography, SIAM Rev. **41**, 85 - 101 (1999).

[8] Cheney, M.: A mathematical tutorial on Synthetic Aperture Radar, SIAM Rev. **43**, 301 - 312 (2001).

[9] Colton, D. and Kress, R.: Inverse Acoustic and Electromagnetic Scattering Theory. Springer, 1992.

[10] Deans, S. R.: The Radar Transform and some of its Application. Wiley 1983.

[11] Epstein, C. L.: Introduction to the Mathematics of Medical Imaging. Prentice Hall 2003.

[12] Fink, M.: Time-reversal of ultrasonic fields - Part 1: Basic principles, IEEE Trans. Ultrasonic Ferroelectr. Freq. Control **39**, 555 - 567 (1992).

[13] Fourmont, K.: Non-equispaced fast Fourier transform with applications to tomography, J. Fourier Anal. Appl. **9**, 431 - 450 (2003).

[14] Herman, G. T.: Image Reconstruction from Projections: The Fundamentals of Computerized Tomography. Academcic Press, New York 1980.

[15] Kak, A. C. and Slaney, M.: Principles of Computerized Tomography Imaging. IEEE Press, New York (1987). Reprinted as SIAM Classics in Applied Mathematics, Philadelphia 2001.

[16] Kirsch, A.: The factorization method for a class of inverse elliptic problems, Math. Nachr. **278**, 258 - 277 (2005).

[17] Klein, J.: Mathematical problems in synthetic aperture radar, Dissertation, Fachbereich Mathematik und Informatik, Universität Münster, Münster 2004.

[18] Klyubina, O.: Asymptotic Methods in Ultrasound Tomography. Thesis, Fachbereich Mathematik und Informatik, Münster 2005.

[19] Morneburg, H. (ed.): Bildgebende Verfahren für die Medizinische Diagnostik. Publis MCD Verlag, Erlangen 1995

[20] Mueller, I. L., Siltanen, S. and Isaacson, D.: A direct reconstruction algorithm for electrical impedance tomography, IEEE Trans. Med. Imag. **21**, 555 - 559 (2002).

[21] Nachman, A. I.: Global uniqueness for a two-dimensional inverse boundary value problem, Ann. of Math. **143**, 71 - 96 (1996).

[22] Natterer, F.: The Mathematics of Computerized Tomography. Wiley - Teubner, New York - Leipzig 1986. Reprinted as SIAM Classics in Applied Mathematics, Philadelphia 2001.

[23] Natterer, F.: Ultrasonic image reconstruction via plane wave stacking, Preprint, Institut für Numerische und Angewandte Mathematik, Münster 2005.

[24] Natterer, F.: Errorestimates for the Born approximation, Inverse Problems **20**, 447 - 452 (2004).

[25] Natterer, F. and Ritman, E. L.: Past and Future Directions in X-Ray Computed Tomography (CT), International Journal of Imaging Systems and Technologie **12**, 175 - 187 (2002).

[26] Natterer, F. and Wübbeling, F.: Mathematical Methods in Image Reconstruction. SIAM, Philadelphia 2001.

[27] Natterer, F. and Wübbeling, F.: Scatter correction in PET based on transport models, Technical Report 14/04-N, Angewandte Mathematik und Informatik, Münster 2004

[28] Natterer, F. and Wübbeling, F.: Marching schemes for inverse acoustic scattering problems, Numerische Mathematik **100**, 697 - 710 (2005).

[29] Natterer, F. and Wübbeling, F.: A propagation-backpropagation method in ultrasound tomography, Inverse Problems **11**, 1225 - 1232 (1995).

[30] Nolan, C. I. and Cheney, M.: Synthetic aperture inversion, Inverse Problems **18**, 221 - 236 (2002).

[31] Novikov, R. G.: Formulae and equations for finding scattering data from the Dirichlet-to-Neumann map with nonzero background potential, Inverse Problems **21**, 257 - 270 (2005).

[32] Novikov, R. G.: An inversion formula for the altenuated X-ray transform, Ark. Mat **40**, 145 - 167 (2002).

[33] Palamodov, V.: Reconstructive Integral Geometry. Birkhäuser Verlag, Basel 2004.

[34] Palamodov, V. P.: Stability in diffraction tomography and a nonlinear "basic theorem", J. Anal. Math. **91**, 247 - 268 (2003).

[35] Papanicolaou, G.: Mathematical problems in geophysical wave propagation, in: Documenta Mathematica, Extra Volume ICM 98, 241 - 265 (1998).

[36] Rose, I. H., Cheney, M. and DeFacio, B.: The connection between time-frequency-domain three-dimensional inversed scattering methods, Math. Phys. **25**, 2995 - 3000 (1984).

[37] Sylvester, I. and Uhlmann, G.: A global uniqueness theorem for an inverse boundary value problem, Ann. of Math. **125**, 153 - 169 (1987)

[38] Symes, W. W. and Carazzone, I. I.: Velocity inversion by differential semblence optimisation, Geophysics **56**, 654 - 663 (1991).

[39] Tarantola, A.: Inversion of travel times and seismic waveforms, in: Nolet (ed.): Seismic Tomography. D. Reidel, Boston 1987.

[40] Welch, A., Clack, R., Natterer, F. and Gullberg, G. T.: Towards accurate attenuation correction in SPECT without transmission scan, IEEE Trans. Med. Imag. **16**, 532-541 (1997).